

FIRST RESULTS FROM FAINT INFRARED GRISM SURVEY (FIGS): FIRST SIMULTANEOUS DETECTION OF LYMAN- α EMISSION AND LYMAN BREAK FROM A GALAXY AT $Z=7.51$

V. TILVI¹, N. PIRZKAL², S. MALHOTRA¹, S. L. FINKELSTEIN³, J. E. RHOADS¹, R. WINDHORST¹, N. A. GROGIN², A. KOEKEMOER², N. L. ZAKAMSKA^{4,5}, R. RYAN², L. CHRISTENSEN⁶, N. HATHI⁷, J. PHARO¹, B. JOSHI¹, H. YANG¹, C. GRONWALL^{8,9}, A. CIMATTI¹⁰, J. WALSH¹¹, R. O'CONNELL¹¹, A. STRAUGHN¹³, G. OSTLIN¹⁴, B. ROTHBERG¹⁵, R. C. LIVERMORE³, P. HIBON¹⁶, AND JONATHAN P. GARDNER¹³

ABSTRACT

Galaxies at high redshifts provide a valuable tool to study *cosmic dawn*, and therefore it is crucial to reliably identify these galaxies. Here, we present an unambiguous and first simultaneous detection of both the Lyman- α emission and the Lyman break from a $z = 7.512 \pm 0.004$ galaxy, observed in the Faint Infrared Grism Survey (FIGS). These spectra, taken with G102 grism on Hubble Space Telescope (HST), show a significant emission line detection (6σ) in two observational position angles (PA), with Lyman- α line flux of $1.06 \pm 0.19 \times 10^{-17}$ erg s⁻¹cm⁻². The line flux is nearly a factor of four higher than in the archival MOSFIRE spectroscopic observations. This is consistent with other recent observations implying that ground-based near-infrared spectroscopy underestimates total emission line fluxes, and if confirmed, can have strong implications for reionization studies that are based on ground-based Lyman- α measurements. A $4\text{-}\sigma$ detection of the NV line in one PA also suggests a weak Active Galactic Nucleus (AGN), and if confirmed would make this source the highest-redshift AGN yet found. These observations from the *Hubble Space Telescope* thus clearly demonstrate the sensitivity of the FIGS survey, and the capability of grism spectroscopy to study the epoch of reionization.

1. INTRODUCTION

To gain a complete understanding of the early universe, it is crucial to reliably identify high-redshift galaxies, because the formation and evolution of the earliest galaxies and the ionization of the intergalactic medium (IGM) during the epoch of reionization are deeply intertwined. The current consensus is that the IGM is mostly

ionized at $z < 7$ (Fan et al. 2002; Malhotra & Rhoads 2004), and therefore, the process of reionization must have occurred at $z \gtrsim 7$, where the IGM is expected to be significantly neutral. This is also consistent with recent Planck results (Planck Collaboration 2015), which find an electron scattering optical depth equivalent to an instantaneous reionization event at $z \approx 8.8$.

Lyman- α emission from star-forming galaxies provides a unique probe of reionization. This is because Lyman- α flux is attenuated by the neutral hydrogen in the IGM as Lyman- α photons are resonantly scattered out of the line of sight when passing through a neutral IGM. This should result in a decrease in Lyman- α emitting galaxy counts at $z > 6$ (Rhoads & Malhotra 2001; Hu et al. 2002; Malhotra & Rhoads 2004). In addition to being a probe of reionization, galaxies in the early universe likely contributed significantly to the reionization process (Oesch et al. 2010; McLure et al. 2010; Finkelstein et al. 2012; Robertson et al. 2013; Finkelstein et al. 2015; Bouwens et al. 2015). Furthermore, the $z > 6$ universe provides the best chance to discover pristine galaxies (Sobral et al. 2015), and therefore identification of high- z galaxies is essential to gain a critical insight into the early universe.

In recent years, significant progress has been made in identifying hundreds of galaxy candidates at $z > 7$, using extremely deep imaging observations from the *Hubble Space Telescope* (HST; e.g., Finkelstein et al. 2015; Bouwens et al. 2015, and references therein). These galaxy candidates, referred to as ‘Lyman-break’ galaxies (LBGs), are primarily selected based on the Lyman- α break at 1216 Å caused by the intervening neutral hydrogen in the IGM. While there have been several spectroscopic followup observations of $z > 7$ LBGs, only a handful of galaxies have yielded spectroscopic redshifts via detection of either the Lyman- α emission line (e.g.,

¹ School of Earth & Space Exploration, Arizona State University, Tempe, AZ. 85287, USA

² Space Telescope Science Institute, Baltimore, MD. 21218, USA

³ Department of Astronomy, The University of Texas at Austin, Austin, TX. 78712, USA

⁴ Deborah Lunder and Alan Ezekowitz Founders’ Circle Member, Institute for Advanced Study, Einstein Dr., Princeton, NJ 08540, USA

⁵ Department of Physics & Astronomy, Johns Hopkins University, Bloomberg Center, 3400 N. Charles St., Baltimore, MD 21218, USA

⁶ 1 Dark Cosmology Centre, Niels Bohr Institute, University of Copenhagen, Juliane Maries Vej 30, 2100 Copenhagen, Denmark

⁷ Aix Marseille Universit, CNRS, LAM (Laboratoire d’Astrophysique de Marseille) UMR 7326, 13388, Marseille, France

⁸ Department of Astronomy and Astrophysics, The Pennsylvania State University, University Park, PA 16802, USA

⁹ Institute for Gravitation and the Cosmos, The Pennsylvania State University, University Park, PA 16802, USA

¹⁰ Dipartimento di Fisica e Astronomia, Università di Bologna, Alma Mater Studiorum, viale Berti Pichat 6/2, I-40127 Bologna, Italy

¹¹ European Southern Observatory, Karl-Schwarzschild Strasse 2, D-85748 Garching, Germany

¹² Department of Astronomy, University of Virginia, Charlottesville, VA 22904-4325, USA

¹³ Astrophysics Science Division, Goddard Space Flight Center, Code 665, Greenbelt, MD 20771, USA

¹⁴ Department of Astronomy, Stockholm University, Oscar Klein Center, AlbaNova, Stockholm SE-106 91, Sweden

¹⁵ Large Binocular Observatory, Tucson, AZ 85721, USA

¹⁶ Gemini South Observatory, Casilla 603, La Serena, Chile

Vanzella et al. 2011; Ono et al. 2012; Shibuya et al. 2012; Finkelstein et al. 2013; Schenker et al. 2014; Oesch et al. 2015; Zitrin et al. 2015) or the Lyman-break (Watson et al. 2015; Oesch et al. 2016).

Galaxy searches at $z > 7$ have also been carried out using a narrow-band imaging technique in which galaxies are preselected to have a strong Lyman- α line (known as Lyman- α emitting galaxies; LAEs). This technique has been successfully employed to identify many LAE candidates out to $z > 7.5$ (e.g., Hiben et al. 2010; Tilvi et al. 2010; Clément et al. 2012; Krug et al. 2012)

Despite spectroscopic successes at $z < 7$, spectroscopic confirmations of a large sample of galaxies at $z > 7$ has been challenging. Recent studies, based on spectroscopic observations of $z > 7$ galaxies, have claimed a precipitous drop in the observed number of Lyman- α emitting galaxies among LBGs (Caruana et al. 2012; Treu et al. 2013; Tilvi et al. 2014; Faisst et al. 2014; Schenker et al. 2014). However, it is not obvious whether the dominant factor behind the non-detection of expected Lyman- α emission is due to small-number statistics, evolving galaxy properties, an observational selection bias, or increasing neutral hydrogen at $z > 7$. These issues are further complicated by the presence of abundant atmospheric night-sky lines at near-infrared wavelengths, contaminating emission lines in the ground-based spectra.

Fortunately, many of the above issues can be circumvented using space-based slitless grism spectroscopy (e.g., Malhotra et al. 2005; Brammer et al. 2012; van Dokkum et al. 2013; Schmidt et al. 2014; Treu et al. 2015) because it eliminates the near-infrared atmospheric contamination. Recently, Schmidt et al. (2016) have found several $z > 7$ candidates using the grism data obtained from the Grism Lens-Amplified Survey from Space (Treu et al. 2015). Furthermore, spectroscopic redshifts have been measured using a continuum detection of the Lyman-break (Rhoads et al. 2013; Oesch et al. 2016) even in the absence of a Lyman- α line. This is critical because while there are other emission lines available for measuring redshifts (see e.g., Stark et al. 2016, and references therein), they are much weaker compared to the Lyman- α line, and therefore, continuum Lyman-break detection provides a promising tool to measure spectroscopic redshifts during the epoch of reionization.

Here we present the first results from the Faint Infrared Grism Survey (FIGS; Malhotra et al. [in prep]), currently the most sensitive G102 grism survey. In this paper, we present the G102 slitless grism spectroscopic observations of FIGS_GN1_1292, a $z = 7.51$ galaxy in the GOODS-N (GN1) field, which has a ground-based spectroscopic redshift based on the Lyman- α emission line detection. Using the HST grism observations, this is now the highest redshift galaxy that has simultaneous detection of Ly α emission line and continuum Lyman-break. In §2 we present our observations and spectral extraction. In §3 we present our results, and compare our observations to those from the ground, and in §4 we summarize our conclusions. Throughout this paper, we use AB magnitudes, and Λ -CDM cosmology with $H_0 = 70.0$ km s $^{-1}$ Mpc $^{-1}$, $\Omega_m = 0.27$, and $\Omega_\lambda = 0.73$.

The FIGS survey is a 160-orbit G102 WFC3/grism survey, designed to obtain 40-orbit depth spectroscopic observations in two GOODS-N and two GOODS-S fields. To minimize contamination by overlapping spectra from nearby objects, each field was observed at five different position angles (PA; each at an 8-orbit depth). The 5 PA survey strategy was found to be optimal in minimizing the contamination in the spectra of $z > 6$ sources based on aXesim simulations (see Malhotra et al in preparation). The total exposure time for the 40-orbit GN1 field is 101,100 sec; for the 5 individual PAs the exposure time varied from 19,300 to 21,900 sec. For complete details about the FIGS survey, we refer the reader to Malhotra et al (in preparation).

2.1. 2-Dimensional Spectral Extraction

We used the grism extraction software package aXe¹⁷ (Pirzkal et al. 2001, Kümmel et al. 2009) to extract individual sources. The method is similar to that of the GRISM ACS Program for Extragalactic Surveys (GRAPES; Pirzkal et al. 2004), but includes additional steps necessary to handle the HST WFC3 infrared data of FIGS.

First, a master catalog of sources was generated using deep mosaics from the CANDELS survey (Koekemoer et al. 2011; Grogin et al. 2011) in the z, J, and H bands. These mosaics also served as our absolute astrometric reference points for the FIGS F105W direct images and the associated dither G102 exposures. They also allowed us to include the colors of sources when computing spectral contamination. Special care was taken to subtract the varying backgrounds from the individual WFC3 exposures. This includes the HeI varying background (Brammer et al 2014¹⁸, Sabbi et al 2015¹⁹) and the zodiacal light background levels, and allowed for the use of up-the-ramp fitting to remove cosmic rays from individual WFC3 exposures. 2-dimensional spectra were then extracted and combined at each position angle using the aXeDrizzle feature of aXe, which also removes the sky background. The end product is a set of multi-extension FITS files that each contain the spectrum of the science object (drizzled to the native pixel scale of 0".128 per pixel, with a linearized wavelength scale), an error estimate, a spectral contamination model, and an effective exposure map. Details of the FIGS pipeline are given in Pirzkal et al. (in preparation).

2.2. 1D Extraction

We extracted 1D spectra of FIGS_GN1_1292 from the 2D multi-extension FITS file by summing all pixels in the spatial direction (3 pixels wide) and collapsing it to a single pixel at each wavelength. Based on our 3 and 5 pixel extraction widths, we found that 3-pixel extraction width yields maximum signal-to-noise (S/N) ratio for the Lyman- α line, and therefore, in this study we use 3-pixel (0.384") extraction width, which is also well matched to the FWHM (0.36") of FIGS_GN1_1292. To convert 1D spectra from counts/sec to physical units (erg s $^{-1}$ cm $^{-2}$ Å $^{-1}$), we

¹⁷ <http://axe-info.stsci.edu/>

¹⁸ ISR WFC3 2014-03

¹⁹ WFC3 ISR 2015-07

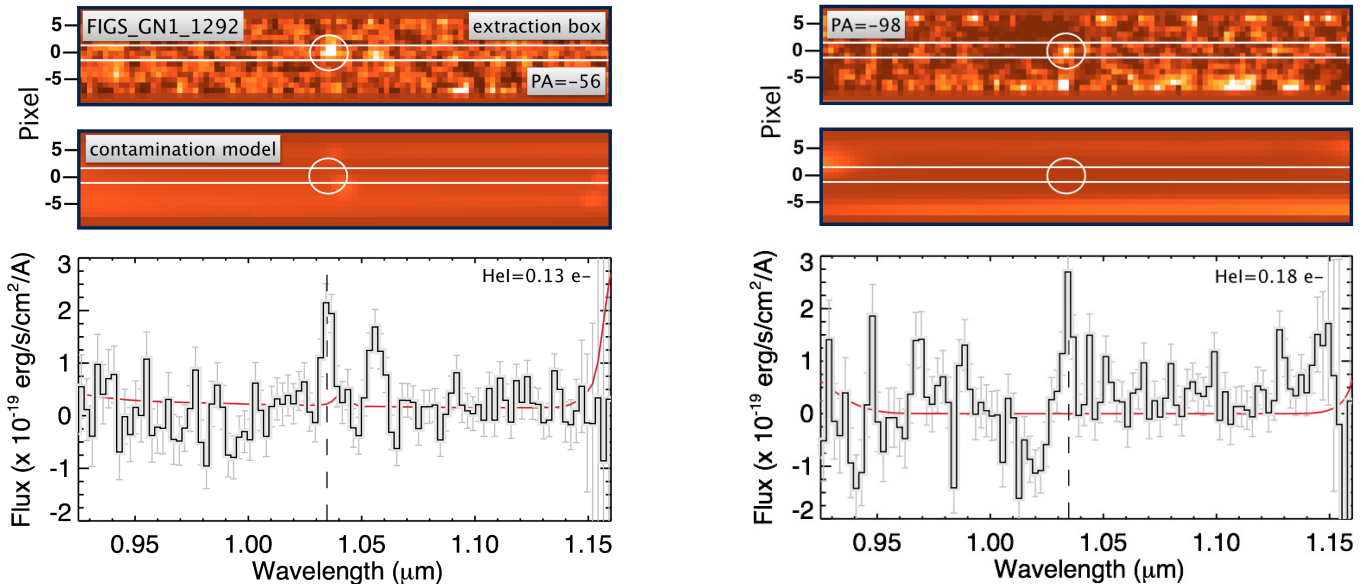


FIG. 1.— Spectra of FIGS_GN1_1292 in two PAs used in this work. Left: The top panel shows the 2D spectrum in PA=−56 (not corrected for contamination). The middle panel shows the contamination model, while the bottom panel shows the contamination-corrected 1D spectrum. The red line in the bottom panel shows the contamination level. The rectangular region in the 2D spectrum is the extraction area (3 pixels wide), and the circle represents the detected emission line. A second possible emission feature is seen near $1.055\mu\text{m}$ in this PA. Possible interpretations of this feature are discussed in section 3.2. The HeI sky-background (noted in legend) significantly varies among different PAs, decreasing the sensitivity of spectra (see §3.1 for details). Right: Same as left panels but for the PA=−98 observations.

used the following conversion: $\text{flux} [\text{erg s}^{-1} \text{cm}^{-2} \text{\AA}^{-1}] = \text{flux} [\text{counts/sec}]/\text{sensitivity}/\text{dispersion}$, where the sensitivity comes from the sensitivity function²⁰ provided for the WFC3 grism, and the dispersion is the wavelength dispersion at each wavelength. Our preliminary estimates of the survey depth, based on inserting and recovering simulated sources, reaches the expected line flux limit of $9 \times 10^{-18} \text{ erg s}^{-1} \text{cm}^{-2}$ (3σ) for a single PA.

3. RESULTS AND DISCUSSION

3.1. Line Detection

As can be seen in Figure 1, the emission line is clearly visible in both the 2D and 1D spectra in two PAs. This object has a previous ground-based Keck/MOSFIRE spectroscopic redshift of $z = 7.5078 \pm 0.0004$, based on a faint Lyman- α line detection (Finkelstein et al. 2013).

For this galaxy, while there are five different PAs available from the FIGS data, three of the PAs (Figure 2) are significantly affected by varying HeI background (noted in legends). The three PAs where the line is not detected have HeI backgrounds that are nearly $10\times$ higher. This elevated HeI background²¹ does not vary significantly during the FIGS grism integrations, thanks to our survey design where we obtained direct imaging observations at the beginning or end of each orbit when the HeI background was expected to be highest and most variable. Thus we do not gain in S/N by discarding individual grism readouts. Therefore, to increase the signal-to-noise ratio in the stacked spectrum (§3.3), we use data from only two PAs in this study.

3.2. Possible Detection of NV

In PA=−56, in addition to the Lyman- α line at $\lambda \sim 1.03\mu\text{m}$, there is another significant line ($f_\lambda = 0.91 \pm 0.21 \times 10^{-17} \text{ erg s}^{-1} \text{cm}^{-2}$) at $\lambda \sim 1.055\mu\text{m}$, with a spatial offset of $\sim 0''.1$, perpendicular to the dispersion direction. This line, however, is not detected in PA=−98. Our careful inspection of 2D spectrum in PA=−56 did not yield any 0th, 1st, or 2nd order contamination from other sources; our contamination models already include contamination from these orders. Furthermore, inspection of 1D spectra of contaminating sources do not show any strong emission line that could potentially produce the tentative NV line at $\lambda \sim 1.055\mu\text{m}$ in PA=−56.

Inspection of the ground-based spectrum found a marginal detection (2.5σ) at $\lambda \sim 1.055\mu\text{m}$, however with a slightly larger spatial offset from the Lyman- α axis. Thus, based on the offsets seen in the 2D grism and MOSFIRE spectra and the RGB image (Figure 3), it is possible that this line is NV($\lambda 1240$), a high ionization line, and a signature of an (weak) Active Galactic Nucleus (AGN; e.g., Hamann & Ferland 1999), off-centered from the Lyman- α emitting region. Furthermore, it is also possible that the NV emission is enhanced via resonant scattering of Lyman- α photons (e.g., Wang et al. 2010). Such off-axis emission from AGN reflection clouds has been seen before at lower redshifts (Windhorst et al. 1998), and it is argued that such off-axis emission could be missed in spectroscopy due to different position angles in both ground-based and space-based spectroscopy.

In addition, we performed simulations by inserting and recovering artificial lines in the 2D spectra, and found that about 5% of the times, a line as bright as the tentative NV line will remain undetected at $< 1\sigma$ significance. Stronger conclusions will likely depend on deeper G141 grism data in the GN1 field. However, if the observed NV line is real, that would make this the

²⁰ WFC3.IR.G102.1st.sens.1.fits

²¹ It is possible that our background noise is underestimated, however this does not change our conclusions in this paper.

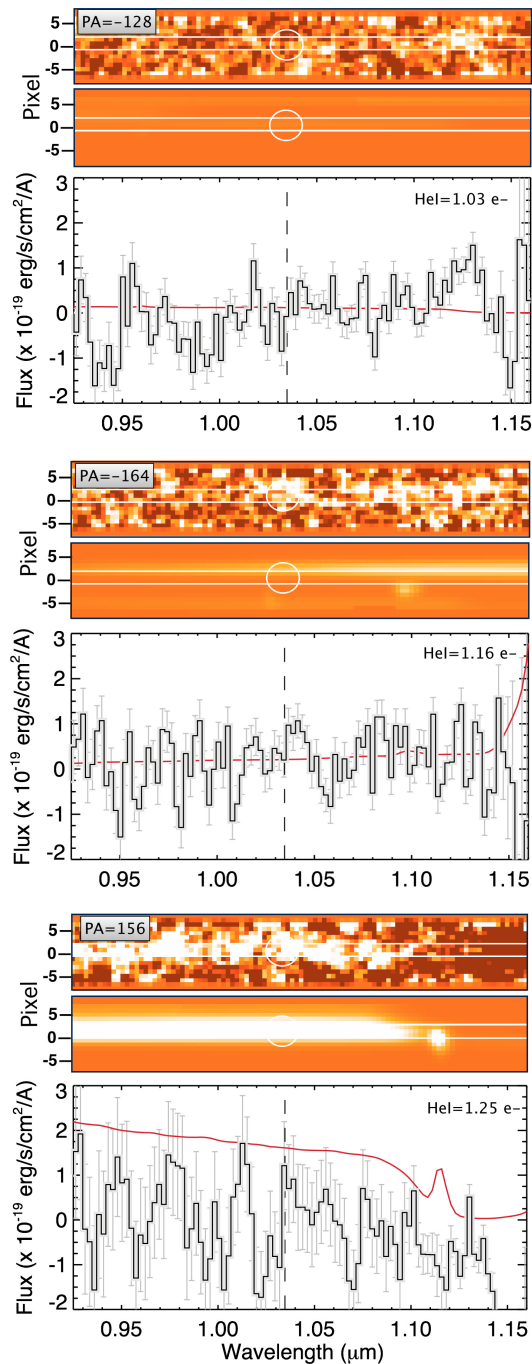


FIG. 2.— Same as Figure 1 except for the remaining three PAs where the Lyman- α line is not detected. The vertical dashed line shows the position of the expected Lyman- α line.

highest-redshift AGN, and would support the idea that the (weak) AGNs might help clear the surrounding neutral hydrogen around galaxies during the epoch of reionization, making them visible in the Lyman- α emission.

3.3. Emission Line Properties

To increase the signal-to-noise ratio of FIGS_GN1_1292 spectra, we combined the two PAs (from Figure 1) to get average 2D and 1D spectra (Figure 4). As can be seen the emission line appears well-detected in both 2D and 1D, and the emission line

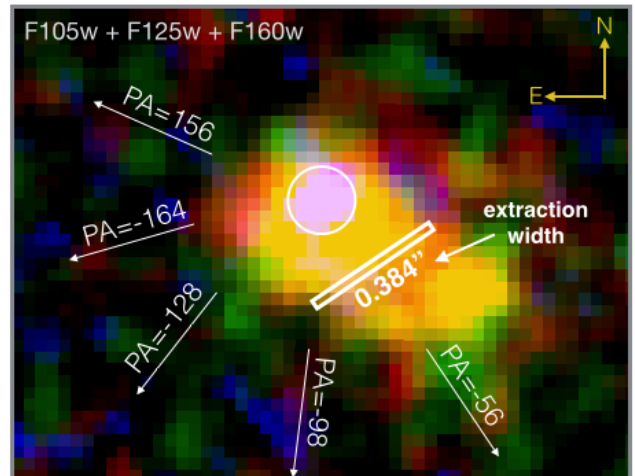


FIG. 3.— RGB composite of FIGS_GN1_1292 using HST/WFC3 broadband images. The off-centered white region enclosed within the white circle is likely the source of the Lyman- α emission. The white rectangular box shows the spectral extraction width ($0''.384$). In the 2D spectrum (Figure 1; left panel) there is a possible detection of NV. If real, this is likely coming from a weak AGN at the center of the galaxy.

wavelength (shown with vertical dashed line) matches very well with the ground-based spectrum.

Alternative explanations for the $\lambda = 1.0347 \mu\text{m}$ line are strongly disfavored. H α is ruled out by the spectral break in the FIGS spectrum while the [OIII] doublet is ruled out by the break *and* by the absence of a [OIII] $\lambda 4959$ line in the MOSFIRE spectrum (Finkelstein et al. 2013). The [OII] $\lambda 3727$ doublet is hardest to rule out. Line asymmetry would be useful in principle, but the MOSFIRE spectrum overlaps a night sky line, precluding reliable asymmetry measurement (Finkelstein et al. 2013), and the FIGS data lack the needed spectral resolution. We highly disfavor the line being [OII] emission due to non-detection of the [OIII] emission line at $\lambda \sim 1.39 \mu\text{m}$ in the archival G141 grism data, and therefore favor this line being Lyman- α emission from a $z = 7.51$ galaxy.

To measure the grism line properties we used a Gaussian fitting function (MPFIT function in IDL) to the 1D spectrum, shown in Figure 4 (middle panel). We measured the Lyman- α equivalent width ($W_{\text{Ly}\alpha}$; the ratio of emission line flux to the continuum flux density) using the average continuum flux density between $\lambda = 1.07 \mu\text{m}$ and $\lambda = 1.14 \mu\text{m}$ (Figure 4), which yields $f_{\lambda} = 2.52 \pm 0.59 \times 10^{-20} \text{ erg s}^{-1} \text{ cm}^{-2} \text{ \AA}^{-1}$. Combining this measurement with the Lyman- α line flux, we get rest-frame $W_{\text{Ly}\alpha} = 49.3 \pm 8.9 \text{ \AA}$. Other physical properties are listed in Table 1.

3.4. Comparison of Keck/MOSFIRE Spectroscopic and HST Grism Spectra

The bottom panel in Figure 4 shows the Keck/MOSFIRE ground-based spectrum of this source. The MOSFIRE spectrum (shown in gray) is contaminated by several OH sky-line residuals, some of which are even brighter than the Lyman- α line itself, making it difficult to observe in the near-infrared part of the spectrum from the ground. The emission line at $\lambda = 1.0343 \mu\text{m}$ (marked by the vertical dashed line) is partly contaminated by a night-sky line. The

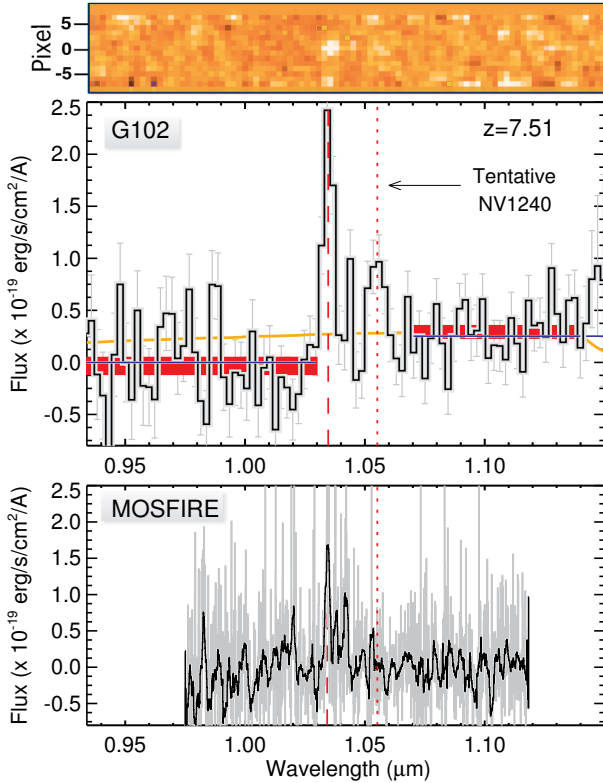


FIG. 4.— Top: the average of two contamination-free PAs from Figure 1 for FIGS_GN1_1292 in the GN1 field. The middle panel shows 1D contamination-corrected spectrum, extracted using 3 pixels-wide aperture. As can be seen, the Lyman- α emission line is clearly visible in both 2D and 1D spectra, with wavelength $\lambda = 1.0347 \pm 0.005 \mu\text{m}$, consistent with the ground-based Keck/MOSFIRE spectroscopic detection (bottom panel) from Finkelstein et al. (2013). The orange horizontal line shows the sensitivity of G102, normalized to the redder continuum. The MOSFIRE spectrum shown in gray represents native resolution while black line shows a heavily smoothed spectrum. The FIGS HST grism spectrum also shows a clear detection of the continuum (horizontal blue line, and errors from bootstrap technique shown in shaded red region; see §3.5) with 5.6σ significance measured at $\lambda = 1.07 - 1.14 \mu\text{m}$.

space-based grism observations do not suffer from this issue. On the other hand, the MOSFIRE spectrum has a much higher spectral resolution which would potentially allow to distinguish between two closely spaced lines, as well as the shape of the Lyman- α line that tends to be asymmetric at high redshifts. With the G102 grism resolution, we cannot measure the shape of the Lyman- α line.

The emission line wavelength in the FIGS_GN1_1292 spectrum matches very well with the ground-based Keck/MOSFIRE spectroscopic redshift from Finkelstein et al. (2013). There is however, a significant difference in the line flux, in that our grism-measured line flux is ~ 4 times higher than the measurements from the MOSFIRE spectrum. A similar discrepancy has been seen before, in Masters et al. (2014), where they found that the *HST*/WFC3 G141 grism line fluxes were higher by a factor of 2 – 4 compared to the ground-based Magellan/FIRE measurements. A similar flux comparison between *HST*/ACS grism and LDSS3 found a scatter of about 0.5 to 2, however with no systematics (Xia et al. 2011). In this study, while the origin of these discrepan-

TABLE 1
PROPERTIES OF FIGS_GN1_1292

	Grism	MOSFIRE ^a
RA, DEC	12:36:37.913 +62:18:08.60	
$\lambda_{Ly\alpha}$ (μm)	1.0347 ± 0.005	1.0343 ± 0.0004
$z_{Ly\alpha}$	7.512 ± 0.004	7.5078 ± 0.0004
$z_{Lyman-break}$	7.512	—
$f_{Ly\alpha}$ ($10^{-17} \text{ erg s}^{-1} \text{ cm}^{-2}$)	1.06 ± 0.19	0.264 ± 0.034
$f_{\lambda > 1.07 \mu\text{m}}$ ($10^{-20} \text{ erg s}^{-1} \text{ cm}^{-2}$)	2.52 ± 0.59	—
$W_{Ly\alpha}(rest)$ (\AA)	49.3 ± 8.9	7.5 ± 1.5
FWHM (\AA)	44 ± 9	7.7 ± 1
$L_{Ly\alpha}$ ($10^{42} \text{ erg s}^{-1}$)	7.1 ± 1.3	1.77 ± 0.36
Y_{F105W} (mag)	26.7 ± 0.2	—
Lyman-break significance (σ) ^b	4.8	—

^a From Finkelstein et al. (2013).

^b Based on bootstrap technique (see §3.5).

cies is not entirely clear, possible contributing factors include underestimation of contamination in grism spectra, slit-losses in ground-based spectroscopic measurements, underestimation of fluxes due to presence of atmospheric lines and much higher resolution of ground-based spectrographs, and uncertainties in the absolute flux calibration. For FIGS_GN1_1292 the grism flux calibrations seem not to be at fault since they agree with the flux measurements from broadband images. Whatever the cause, if emission line fluxes at near-IR wavelengths from ground-based measurements are confirmed to be underestimates, it would reduce the apparent strong redshift evolution in the Lyman- α equivalent width distribution. Firmer conclusions would benefit from a larger $z > 7$ galaxy sample. Furthermore, to minimize the systematic errors in the Lyman- α equivalent width distribution, ideally, sample galaxies should be detected in both Lyman- α emission and the continuum, as in the case of FIGS_GN1_1292 (see below).

3.5. Lyman break detection

As mentioned earlier, there was no continuum break detected in the ground-based spectroscopic observations (Finkelstein et al 2013) of FIGS_GN1_1292, due to shallower continuum sensitivity of MOSFIRE observations. Using G102 grism observations of FIGS_GN1_1292, we have detected the continuum Lyman-break, making this the second-most distant galaxy with a spectroscopic continuum detection (cf. Oesch et al. 2016). Figure 4 shows the 1D spectrum of FIGS_GN1_1292, where the flux redward of the Lyman- α line is clearly higher than the blueward flux. To check for any artificial break created by the G102 sensitivity (Figure 4), we performed aXesim simulations using flat input spectrum, with a range of continuum magnitudes covering FIGS_GN1_1292. We conclude that the observed Lyman-break is not caused by the declining sensitivity function of G102.

The horizontal blue lines in Figure 4 show the median flux measured using the bootstrap technique where we resampled and replaced a flux value, and remeasured the median flux value. Repeating this simulation 5000 times yields a median flux value of $f_{\lambda} = 0.00^{+0.49}_{-1.16} \times 10^{-20} \text{ erg s}^{-1} \text{ cm}^{-2}$ and $f_{\lambda} = 2.52^{+1.02}_{-0.21} \times 10^{-20} \text{ erg s}^{-1} \text{ cm}^{-2}$, on the blue and red side respectively. These values yield Y_{F105W} bandpass magnitude

of 26.7 ± 0.2 mag, in agreement with the measured magnitude from the imaging data, with $Y_{F105W} = 26.4 \pm 0.2$ mag.

To measure the Lyman-break significance in the presence of asymmetric error bars, we use the upper error bar on the blue flux, and lower error bar on the red continuum flux. This yields a Lyman-break significance of 4.8σ . In addition to using bootstrap technique, we directly measured the median fluxes on blue and red side. This yields $f_{\lambda} = 0.00 \pm \times 10^{-20}$ erg s $^{-1}$ cm $^{-2}$ and $f_{\lambda} = 2.52 \pm 0.59 \times 10^{-20}$ erg s $^{-1}$ cm $^{-2}$, on the blue and red side respectively. This yields Lyman-break significance of 2.7, somewhat lower than the bootstrap measurement, which is likely due to overestimated errors due to non-normal flux distribution. Thus, based on the bootstrap measurements, FIGS_GN1_1292 is currently the most-distant galaxy that has been spectroscopically confirmed using both the Lyman- α line and the Lyman-break.

4. SUMMARY

Here we presented grism spectroscopy of FIGS_GN1_1292, the first object at $z > 7$ that has

been spectroscopically confirmed using both the Lyman- α line and the Lyman-break— prior to this, $z > 7$ galaxies have been confirmed using either Lyman- α emission line or the Lyman-break detection. Our accurate redshift measurement based on the continuum break detection demonstrates the value of FIGS and similar surveys for continuum observations. This is crucial because as we probe the epoch of reionization, we expect Lyman- α emission to attenuate, and therefore redshift measurements from continuum break becomes critical. Thus, our successful identification of a galaxy in the reionization epoch motivates planning for even more sensitive space-based grism surveys from upcoming missions including the *James Webb Space Telescope* and the *Wide Field Infrared Survey Telescope*.

We thank the referee for very useful feedback that improved this manuscript. This work is based on observations taken by the FIGS program (GO 13779) with the NASA/ESA HST, which is operated by the Association of Universities for Research in Astronomy, Inc., under NASA contract NAS5-26555. RAW acknowledges support from NASA JWST Interdisciplinary Scientist grant NNX14AN10G from GSFC.

REFERENCES

- Bouwens, R. J., Illingworth, G. D., Oesch, P. A., et al. 2015, *ApJ*, 811, 140
- Brammer, G. B., van Dokkum, P. G., Franx, M., et al. 2012, *ApJS*, 200, 13
- Caruana, J., Bunker, A. J., Wilkins, S. M., et al. 2012, *MNRAS*, 427, 3055
- Clément, B., Cuby, J.-G., Courbin, F., et al. 2012, *A&A*, 538, A66
- Faisst, A. L., Capak, P., Carollo, C. M., Scarlata, C., & Scoville, N. 2014, arXiv:1402.3604
- Fan, X., Narayanan, V. K., Strauss, M. A., et al. 2002, *AJ*, 123, 1247
- Finkelstein, S. L., Papovich, C., Salmon, B., et al. 2012, *ApJ*, 756, 164
- Finkelstein, S. L., Papovich, C., Dickinson, M., et al. 2013, *Nature*, 502, 524
- Finkelstein, S. L., Ryan, R. E., Jr., Papovich, C., et al. 2015, *ApJ*, 810, 71
- Grogin, N. A., Kocevski, D. D., Faber, S. M., et al. 2011, *ApJS*, 197, 35
- Hamann, F., & Ferland, G. 1999, *ARA&A*, 37, 487
- Hibon, P., Cuby, J.-G., Willis, J., et al. 2010, *A&A*, 515, A97
- Hu, E. M., Cowie, L. L., McMahon, R. G., et al. 2002, *ApJ*, 568, L75
- Koekemoer, A. M., Faber, S. M., Ferguson, H. C., et al. 2011, *ApJS*, 197, 36
- Krug, H. B., Veilleux, S., Tilvi, V., et al. 2012, *ApJ*, 745, 122
- Kümmel, M., Walsh, J. R., Pirzkal, N., Kuntschner, H., & Pasquali, A. 2009, *PASP*, 121, 59
- Malhotra, S., & Rhoads, J. E. 2004, *ApJ*, 617, L5
- Malhotra, S., Rhoads, J. E., Pirzkal, N., et al. 2005, *ApJ*, 626, 666
- Masters, D., McCarthy, P., Siana, B., et al. 2014, *ApJ*, 785, 153
- McLure, R. J., Dunlop, J. S., Cirasuolo, M., et al. 2010, *MNRAS*, 403, 960
- Oesch, P. A., Bouwens, R. J., Carollo, C. M., et al. 2010, *ApJ*, 725, L150
- Oesch, P. A., van Dokkum, P. G., Illingworth, G. D., et al. 2015, *ApJ*, 804, L30
- Oesch, P. A., Brammer, G., van Dokkum, P. G., et al. 2016, *ApJ*, 819, 129
- Ono, Y., Ouchi, M., Mobasher, B., et al. 2012, *ApJ*, 744, 83
- Pirzkal, N., Collodel, L., Erben, T., et al. 2001, *A&A*, 375, 351
- Pirzkal, N., Xu, C., Malhotra, S., et al. 2004, *ApJS*, 154, 501
- P. A. R. Ade, N. Aghanim, M. Arnaud., et al. 2015, arXiv:1502.01589
- Rhoads, J. E., & Malhotra, S. 2001, *ApJ*, 563, L5
- Rhoads, J. E., Malhotra, S., Stern, D., et al. 2013, *ApJ*, 773, 32
- Robertson, B. E., Furlanetto, S. R., Schneider, E., et al. 2013, *ApJ*, 768, 71
- Schenker, M. A., Ellis, R. S., Konidaris, N. P., & Stark, D. P. 2014, *ApJ*, 795, 20
- Schmidt, K. B., Treu, T., Brammer, G. B., et al. 2014, *ApJ*, 782, L36
- Schmidt, K. B., Treu, T., Bradač, M., et al. 2016, *ApJ*, 818, 38
- Stark, D. P., Ellis, R. S., Charlot, S., et al. 2016, arXiv:1606.01304
- Shibuya, T., Kashikawa, N., Ota, K., et al. 2012, *ApJ*, 752, 114
- Sobral, D., Matthee, J., Darvish, B., et al. 2015, *ApJ*, 808, 139
- Tilvi, V., Rhoads, J. E., Hibon, P., et al. 2010, *ApJ*, 721, 1853
- Tilvi, V., Papovich, C., Finkelstein, S. L., et al. 2014, *ApJ*, 794, 5
- Treu, T., Schmidt, K. B., Trenti, M., Bradley, L. D., & Stiavelli, M. 2013, *ApJ*, 775, L29
- Treu, T., Schmidt, K. B., Brammer, G. B., et al. 2015, *ApJ*, 812, 114
- Vanzella, E., Pentericci, L., Fontana, A., et al. 2011, *ApJ*, 730, L35
- van Dokkum, P., Brammer, G., Momcheva, I., et al. 2013, arXiv:1305.2140
- Wang, H., Wang, T., Yuan, W., et al. 2010, *ApJ*, 710, 78
- Watson, D., Christensen, L., Knudsen, K. K., et al. 2015, *Nature*, 519, 327
- Windhorst, R. A., Keel, W. C., & Pascarella, S. M. 1998, *ApJ*, 494, L27
- Xia, L., Malhotra, S., Rhoads, J., et al. 2011, *AJ*, 141, 64
- Zitrin, A., Labbé, I., Belli, S., et al. 2015, *ApJ*, 810, L12